

XRISM View of the Newly Detected Galactic Source MAXI J1744-294

KAUSHIK CHATTERJEE,¹ SANTANU MONDAL,² BISWARAJ PALIT,³ CHANDRA B. SINGH,¹ SUJOY KUMAR NATH,⁴ MAYUKH PAHARI,⁵ BRAJESH KUMAR,¹ WEI WANG,⁶ AND HSIANG-KUANG CHANG⁷

¹South-Western Institute For Astronomy Research, Yunnan University, University Town, Chenggong, Kunming 650500, China

²Indian Institute of Astrophysics, II Block, Koramangala, Bengaluru 560034, Karnataka, India

³Nicolaus Copernicus Astronomical Center, Polish Academy of Sciences, ul. Bartycka 18, 00-716 Warsaw, Poland

⁴Indian Center for Space Physics, 466 Barakhola, Netaji Nagar, Kolkata 700099, India

⁵Department of Physics, Indian Institute of Technology Hyderabad, Hyderabad, Kandi, 502285 Sangareddy, India

⁶Department of Astronomy, School of Physics and Technology, Wuhan University, Wuhan, People's Republic of China

⁷Institute of Astronomy, National Tsing Hua University, Hsinchu 300044, Taiwan, Republic of China

ABSTRACT

The transient Galactic source MAXI J1744-294 went into an outburst in 2025 for the very first time. We study the spectral properties of this source during this outburst using archival data from the XRISM satellite for both of its Resolve and Xten instruments. We have analyzed the source during one epoch, on March 03, 2025, or MJD 60737, on which XRISM data were available. Using both phenomenological and physical model fitting approaches for continuum emissions, along with line emission and interstellar absorption models, we analyzed the spectral data in the broad 2–10 keV energy band. From our spectral analysis, we have found the existence of multiple iron lines, which are different components of the Fe XXV emission. These line complexes arise from two highly ionized plasmas with ionization rate $\sim 10^3$ erg cm s⁻¹ with distinct turbulent velocities—one broad ($v_{\text{turb}} \approx 2513$ km s⁻¹) from hot gas at the inner accretion disk and one narrow ($v_{\text{turb}} \approx 153$ km s⁻¹) scattered by nearby photoionized gas. The source is a moderately spinning black hole with a spin of 0.63 – 0.70, a mass of $7.9 \pm 2.2 M_{\odot}$, and a disk inclination angle of 19 – 24°. The spectral model fitted parameters suggest that the source is in the soft spectral state. The source is situated in a crowded field near the Galactic center, resulting in a very high hydrogen column density.

Keywords: X-rays: binary stars (1811); black holes (162); Stellar accretion disks (1579); Compact radiation sources (289)

1. INTRODUCTION

Transient compact objects show variability signatures in the spectral and temporal properties during their outburst phases. These properties are strongly correlated with each other across different spectral states (Remillard & McClintock 2006; Chakrabarti et al. 2008; Tetarenko et al. 2016, and references therein). In different spectral states, the appearance and disappearance of timing phenomena like quasi-periodic oscillations, or QPOs have been observed (e.g., Belloni et al. 2002; Casella et al. 2005; Motta et al. 2011; Mondal et al. 2014; Chatterjee et al. 2020, 2024a,b, and references therein). Additionally, jets or outflows are often observed phenomena that leave imprints in different spectral states (Chakrabarti 1999; Dhawan et al. 2000; Sunyaev & Titarchuk 1980; Corbel & Fender 2002; Mondal & Chakrabarti 2021). Therefore, their X-ray spec-

trum can tell us the underlying physical processes responsible for the spectral features.

The observed spectral features mainly come from two distinct regions: one is the inner hot puffed-up region, or so-called corona, and the second component is the cold Keplerian disk. The seed photons from the cold disk produce the blackbody spectrum, and some fraction of these photons are upscattered by the corona and give rise to the hard X-ray radiation (Sunyaev & Titarchuk 1980; Haardt & Maraschi 1993; Chakrabarti & Titarchuk 1995; Done et al. 2007, and references therein). Some of the hard photons from the corona fall back to the disk and come out as the so-called reflection component (George & Fabian 1991; Ross & Fabian 2005) leaving a hump above 10 keV (Ross & Fabian 2005; García & Kallman 2010), which is believed to be the origin of the Fe K fluorescent line around 6.4 keV (Fabian et al. 1989; Pozdnyakov et al. 1983). However, the hump above 10 keV can also be originated by the radiation coming from the bulk motion Comptonization effect in the jet (Titarchuk & Shrader 2005; Mondal & Chakrabarti 2021). All these components of the radiation are very informative in understanding the accretion behavior near the BH due to the

emails.kc.physics@gmail.com, kaushik@ynu.edu.cn (KC)

santanuicsp@gmail.com (SM)

strong gravitational effect, reflected in the Fe-K α line profile (Brenneman & Reynolds 2006; Marinucci et al. 2014). The line can break into a double horn if the accretion disk moves much closer to the BH (Fabian et al. 1989; Iwasawa et al. 1996, and references therein), helping to estimate the spin of the central BH (Li et al. 2005; Mondal et al. 2024, and references therein).

Apart from the Fe-K α line, there could be the presence of other Fe-line components also in the 6.5 – 7 keV energy band. Multiple iron line emissions can be observed, which might be associated with the Galactic diffuse X-ray emission, or it can also be due to the physical conditions of the accreting matter (see Mondal et al. 2021, for numerical simulations). The $\sim 6.6 - 6.7$ keV iron line emission plays a significant role in the context of our Galaxy. The emission line at $\sim 6.6 - 6.7$ keV can be identified as a combination of the 6.63, 6.67, and 6.70 keV lines of Fe XXV ions, which could be produced through the recombination process in the accretion disk corona (Asai et al. 2000). The measurements of these features require high-quality X-ray data. The spectacular resolution of the XRISM (Tashiro et al. 2021) data can reveal these multiple line peaks and their origin.

The new Galactic source MAXI J1744-294 was reported on January 02, 2025 (Kudo et al. 2025; Nakajima et al. 2025; Watanabe et al. 2025) by the Monitor of All-sky X-ray Image or, MAXI (Matsuoka et al. 2009) with a flux level of ~ 250 mCrab. From the follow-up observations of Swift/XRT, two sources were detected near Sgr A*, one of which is consistent with the position of the neutron star low-mass X-ray binary AX J1745.6-2901, while the other one is an uncatalogued target at coordinates 17:45:41.93, -29:00:35 in J2000 coordinates (Heinke et al. 2025). Later on February 06, 2025, *NuSTAR* also confirmed some activity from this new source (Mandel et al. 2025). It was observed on February 11-12, 2025, using *NICER* data by (Jaisawal et al. 2025). They reported the presence of an absorbed power-law along with a disk blackbody component in the 2 – 10 keV energy band with an iron line at 6.6 ± 0.9 keV. The authors reported a high column density of $N_H = (11 \pm 1) \times 10^{22} \text{ cm}^{-2}$. This source is located very close to the Galactic center with (R.A., Dec.) = (266.116 deg, -29.433 deg). For the estimation of flux in the 2–10 keV, Mandel et al. (2025) assumed a distance of 8 kpc. Their estimated spectral parameters are consistent with those of a low-mass black hole X-ray binary in the soft state. Very recently Majumder et al. (2025) analyzed the *IXPE* data of the source and could not detect any polarization signature. Along the same line, Marra et al. (2025) found only $\sim 1.3\%$ polarization degree using *IXPE* data and constrained the disk inclination angle of the source in a broad range of 38–71°. A possible cause may be due to the presence of the soft spectral state, where a significantly low or null detection is favourable for several reasons (see Mondal et al. 2024).

In this work, we have analyzed XRISM spectra for both the *Resolve* and *Xtend* instruments in the 2 – 10 keV energy band of the newly detected Galactic source MAXI J1744-294 during its very first outburst in 2025. We have implemented some phenomenological and physical models for this analysis. In the next section, we describe the data reduction procedure. In §3, we discuss the spectral analysis and results. Finally, we draw our conclusions in §4.

2. DATA REDUCTION

We have used XRISM data from both instruments that observed the source on March 03, 2025 (MJD 60737), for this work. The data reduction procedure is discussed below.

The data of the new Galactic source MAXI J1744-294 is downloaded from the publicly available [HEASARC archive](#). Although level-2 cleaned event files are already present in the downloaded data, we reprocessed the data using the `xpipeline` task for both the *Resolve* and *Xtend* instruments separately. After the production of the level-2 cleaned files, as recommended in the [Quick-Start Guide Version 2.3](#), we used additional screening for pulse rise time, event type, and status. We also excluded the events from pixel number 27, as it is recommended for calibration uncertainties. We use the `XSELECT` task to extract spectra and light curve files for science analysis. Then we use `rslmkrmf`, and `xtdrmf` commands to make response files for the *Resolve* and *Xtend* instruments. We have used the extra-large (XL) type of response file for *Resolve*. Next, using the `xaexpmap` command, we create a standard exposure map for both instruments. Then, we create ancillary response files for both instruments using the `xaarfgen` command. We have also created the non-X-ray background for *Resolve* using the `rslnxbgen` command.

3. SPECTRAL ANALYSIS AND RESULTS

We perform spectral analysis of the newly detected Galactic source MAXI J1744-294 using the processed data for science results. We used `XSPEC` to model the data using both phenomenological and physical models. To account for the continuum emission, we have used combinations of models by using a `disk blackbody`, a `kerrbb`, and a `power-law` model. For the interstellar absorption, we have used the multiplicative absorption model component `tbabs`. Different combinations of those four models can fit the continuum satisfactorily. However, some line features are also present in the spectrum, particularly near the 6.5 – 7 keV energy band. Thus, we added multiple `Gaussian` lines to fit these lines. This model combination is applied to both instruments.

First, we looked at the spectra of both instruments. From panel (a) of [Figure A1](#), one can notice that the multiple line features are present in the 6.5 – 7 keV energy band in the *Resolve* spectrum. In panel (b) of [Figure A1](#), we rebinned the

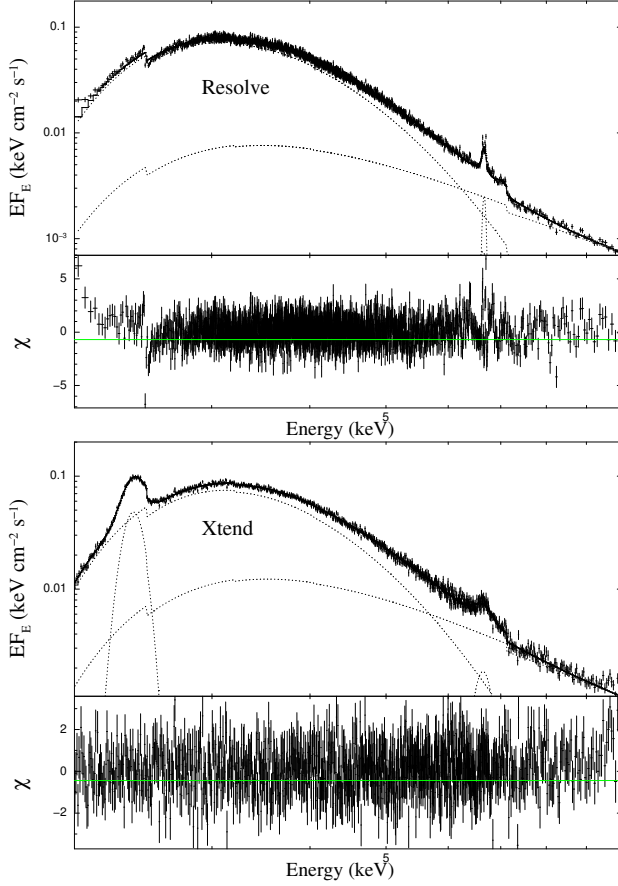


Figure 1. Model-fitted unfolded XRISM spectra for Resolve (top panel) and Xtend (bottom panel) instruments, respectively, by using a combination of `diskbb`, power-law, and Gaussian models.

spectrum in the same energy range for visual clarity. It could be noticed that there are line emission profiles in the Resolve spectrum, which might be related to the Fe-XXV line. We also notice some Fe-line features in the spectrum from Xtend. This could be noticed in panel (a) of Figure A2. However, unlike the Resolve spectrum, this is not clearly resolved in the 6.5 – 7 keV energy band, whether there are multiple line features or not. However, both spectra can certainly show the presence of Fe K lines.

Therefore, first, we try to analyze the continuum spectrum and find a suitable model combination for the continuum emission. For this, we ignored the 6.5 – 7.1 keV energy region for both the instruments. The model combination that is used for the fitting reads as `tbabs*(diskbb + po)`. We found a best-fit continuum for the Resolve spectrum, for which the $\chi^2_{red} = 1.06$. Although this is a very good fit for the continuum, we found there is some absorption nature ~ 2.43 keV, which is shown in panel (d) of Figure A1. For the Xtend spectrum, we found that this combination was not good enough. There is an excess of flux ~ 2.4 keV. The $\chi^2_{red} = 4.284$. By adding another Gaussian (`ga`) model,

we achieve the best fit for the continuum. The model combination reads as `tbabs*(diskbb + po + ga)` for which $\chi^2_{red} = 1.09$, as shown in the panel (d) of Figure A2. After finding the best-fitted continuum model, we included the 6.5 – 7.1 keV energy band in our analysis, which is the main motivation of this work. We found that there is the presence of a triplet line emission in this energy band for the Resolve spectrum. Thus, to get the best fit, we added three `ga` lines, and our best-fitted model combination reads as `tbabs*(diskbb + po + ga[3])` and achieves $\chi^2_{red} = 1.09$. For the Xtend spectrum, as mentioned before, the line features are not resolved properly to identify them as multiple lines. Thus, we only added one `ga` component to the previously achieved best-fitted continuum for Xtend. Thus, our best-fitted model combination reads as `tbabs*(diskbb + po + ga[2])` for which $\chi^2_{red} = 1.07$. The best-fitted unfolded spectra are given in Figure 1. We also performed the spectral analysis by using the `kerrbb` model (Li et al. 2005) by replacing the `diskbb` component. To perform the spectral fitting with this model, we have frozen the distance of the source to 8 kpc (Mandel et al. 2025, though not yet confirmed) and also frozen the hardening factor to 1.7. This model combination reads as `tbabs*(kerrbb + po + ga[3])` for Resolve and `tbabs*(kerrbb + po + ga[2])` for Xtend. With these model combinations, we achieved the best fits with $\chi^2_{red} \sim 1.09$ and 1.07 for the Resolve and Xtend, respectively, which are quite similar to the previous model combinations. However, the use of `kerrbb` model can give preliminary information about the intrinsic properties of the BH. The best-fitted unfolded spectra are shown in Figure 2.

The spectrum from the Resolve instrument showed the presence of multiple line emissions in the 6.5 – 7.1 keV energy band, whereas, for the Xtend, the line components were not resolved properly and looked like a broad Gaussian component. From both the spectral fittings, we found that the N_H was high with values 16.7 ± 0.1 and 17.9 ± 0.1 cm⁻² for Resolve and Xtend, respectively. The source is located in a very crowded region near the Galactic center. Due to its close proximity to the Galactic center, the MAXI satellite could not distinctly resolve the source. The inner disk temperatures (T_{in}) are 0.62 ± 0.04 and 0.60 ± 0.05 keV for Resolve and Xtend, respectively. The `diskbb` model normalizations, $Norm_{diskbb}$ obtained from the best-fits are 6339 ± 269 and 9812 ± 578 for the two instruments. We found that the photon index of the power-law was very high with values $\Gamma \sim 3.2 \pm 0.1$ and 3.3 ± 0.1 , suggesting that the source is in the soft state during this epoch of the outburst. From the Resolve fitting, we find that there was the presence of iron lines at $\sim 6.64, 6.67,$ and 6.99 keV, with widths $100 \pm 30, 35 \pm 3,$ and 100 ± 40 eV, respectively. All the lines have a normalization value of the order of 10^{-4} . These are possibly the multiple components of the Fe-XXV lines, however, subject to a de-

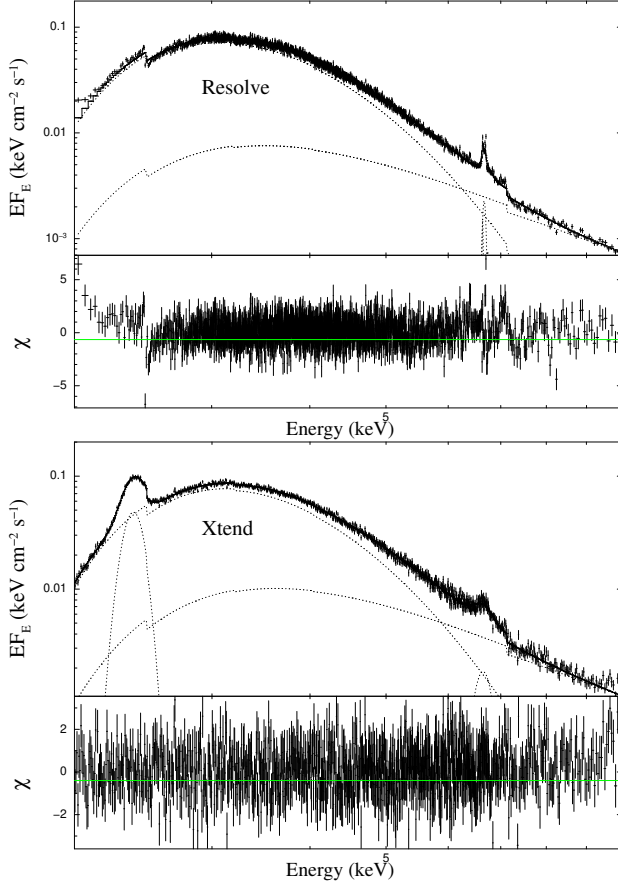


Figure 2. Model-fitted unfolded XRISM spectra for Resolve (top panel) and Xtend (bottom panel) instruments, respectively, by using a combination of *kerbb*, power-law, and Gaussian models.

tailed line profile study. In the Xtend fitting, we found the presence of an iron line at the line energy of 6.64 ± 0.01 keV with a width of 161 ± 17 eV and a normalization of the order of $\sim 10^{-3}$. In the Xtend spectrum, there was the presence of an excess flux at the low energy of $\sim 2.36 \pm 0.02$ keV with a width of 70 ± 2 eV. However, the normalization of this Gaussian was $\sim 0.21 \pm 0.01$. This can be observed in panel (b) of Figure 1. We speculate it could be from the instrumental effect rather than astrophysical. In Table 1, the best-fitted model parameters are listed.

To further estimate the inner-disk radius i.e., the extent of the inner disk, we used the scaling relation, $Norm_{diskbb} = (r_{in}/D_{10})^2 \cos\theta$, where r_{in} , D_{10} , and θ are the inner disk radius (in km), the distance of the source (in units of 10 kpc), and the inclination of the disk (in degrees) to the observer, respectively. However, the above-mentioned r_{in} is subject to some uncertainty (Shimura & Takahara 1995; Kubota et al. 1998). The modified inner disk radius is given by $R_{in} \approx \kappa^2 \xi r_{in}$, where κ and ξ are the hardening factor (Kubota et al. 1998) and inner boundary correction factor (Shimura & Takahara 1995), respectively. According to

Table 1. Values of the spectrally fitted parameters using *tbbabs*, *diskbb*, power-law, and multiple Gaussian models. Column 1 represents the parameters of the phenomenological models used for spectral fitting. Columns 2 & 3 represent the values of those parameters for the Resolve and the Xtend instruments, respectively. The last value of flux is in the units of $10^{-9} \text{ erg cm}^{-2} \text{ s}^{-1}$.

(1) Parameters	(2) Resolve	(3) Xtend
N_H	16.7 ± 0.1	17.9 ± 0.15
T_{in}	0.62 ± 0.04	0.60 ± 0.05
$Norm_{diskbb}$	6339 ± 269	9812 ± 578
Γ	3.2 ± 0.1	3.3 ± 0.1
$Norm$	1.21 ± 0.27	2.46 ± 0.62
E_{Ga1}	6.64 ± 0.11	2.36 ± 0.12
σ_{Ga1}	0.10 ± 0.04	0.07 ± 0.01
$Norm_{Ga1}$	$2e - 4 \pm 4e - 5$	0.21 ± 0.01
E_{Ga2}	6.67 ± 0.17	6.64 ± 0.13
σ_{Ga2}	0.03 ± 0.01	0.16 ± 0.02
$Norm_{Ga2}$	$3e - 4 \pm 4e - 5$	$9e - 4 \pm 8e - 5$
E_{Ga3}	6.99 ± 0.02	-
σ_{Ga3}	0.10 ± 0.04	-
$Norm_{Ga3}$	$1e - 4 \pm 2e - 5$	-
χ^2/DOF	6792/6235	1408/1321
$Flux$	1.04	1.22

them, these two correction factors have values of 1.7 and 0.41, respectively. Thus, the relation becomes $Norm_{diskbb} = (R_{in}/\kappa^2 \xi D_{10})^2 \cos\theta$. So, the correct innerdisk radius (R_{in}) is given as $R_{in} = (\kappa^2 \xi D_{10}) \sqrt{(Norm_{diskbb}/\cos\theta)}$. According to Mandel et al. (2025), we also assume a distance estimate of the source as 8 kpc. Since this source does not have an estimation of the inclination, we assume values of $\theta \sim 20^\circ, 50^\circ$, and 80° for low to high inclination. Given these values, the R_{in} comes out to be $\sim \{78, 94, \text{ and } 184\}$, and $\sim \{97, 118, \text{ and } 229\}$ km for Resolve and Xtend instruments, respectively. Considering the innermost stable circular orbit (ISCO) for the inner-disk radius of a Schwarzschild black hole as a scale factor, the mass of this source varies from $8 - 25 M_\odot$. Such estimates can provide a preliminary understanding of the BH mass. However, to better constrain the physical parameters, data fitting using more realistic models is required.

Therefore, as a further consistency check and to have an estimate of the spin and mass of the source, and the accretion disk inclination, we replaced the *diskbb* component of the model combination with *kerrbb*. From this model fitting, we found that the disk has a low inclination of $\sim 19^\circ - 24^\circ$ and a moderate spin of $\sim 0.63 - 0.70$. This low inclination suggests that the inner disk might be at a distance of $\sim 75 - 100$ km from the central object, obtained from the previous relation. The *kerrbb* model fit determines the mass to be

8.5 – 10.1 M_\odot , which is in agreement with the estimation using `diskbb` model. This further suggests that the object is a black hole and not a neutron star. Considering this mass, it is in good agreement that the inner boundary of the disk has moved inside the $6r_g$ distance from the object, which makes it suitable for iron line emission ($6r_g$ to $30r_g$). The results of this model fitting are given in Table 2.

Table 2. Values of the spectrally fitted parameters using `tbabs`, `kerrbb`, `power-law`, and multiple Gaussian models. Column 1 represents the parameters of the models used for spectral fitting. Columns 2 & 3 represent the values of those parameters for the *Resolve* and the *Xtend* instruments, respectively. The last value of flux is in the units of $10^{-9} \text{ erg cm}^{-2} \text{ s}^{-1}$.

(1) Parameters	(2) Resolve	(3) Xtend
N_H	17.0 ± 0.2	18.1 ± 0.7
spin (a)	0.68 ± 0.02	0.65 ± 0.02
inclination (i)	19.8 ± 0.3	23.4 ± 0.3
Mass (M_{BH})	8.8 ± 0.3	9.6 ± 0.5
Mdd	0.86 ± 0.03	0.87 ± 0.04
$Norm_{kerrbb}$	1.7 ± 0.2	2.27 ± 0.3
Γ	3.2 ± 0.2	3.1 ± 0.6
$Norm$	1.25 ± 0.13	1.62 ± 0.25
E_{Ga1}	6.64 ± 0.14	2.36 ± 0.11
σ_{Ga1}	0.01 ± 0.00	0.07 ± 0.01
$Norm_{Ga1}$	$8e - 5 \pm 2e - 5$	0.22 ± 0.02
E_{Ga2}	6.67 ± 0.32	6.64 ± 0.14
σ_{Ga2}	0.03 ± 0.01	0.16 ± 0.02
$Norm_{Ga2}$	$2e - 4 \pm 4e - 5$	$9e - 4 \pm 8e - 5$
E_{Ga3}	6.72 ± 0.03	-
σ_{Ga3}	0.10 ± 0.01	-
$Norm_{Ga3}$	$2e - 4 \pm 4e - 5$	-
χ^2/DOF	6801/6232	1406/1318
Flux	1.04	1.22

In addition to these models, we have also implemented the physically motivated accretion-ejection based JeTCAF model (Jet in TCAF Mondal & Chakrabarti 2021; Chakrabarti & Titarchuk 1995) by replacing the PL model to estimate the accretion-ejection parameters and the mass of the BH. Since JeTCAF has both hot (corona) and cold (disk) flow components, therefore, it can be fitted to any spectral states whether jet is present or not. Depending on the spectral state, model parameters can be constrained. As the source is in the soft state, that will be imprinted in the jet parameters as well, which can be further verified using this model. There are six parameters in this model, including the mass of the BH if it is not dynamically measured. The parameters are: (i) mass of the BH (M_{BH} in solar mass M_\odot units) (ii) cold Keplerian

disk accretion rate (\dot{m}_d), (iii) hot sub-Keplerian halo accretion rate (\dot{m}_h) (both rates are in Eddington rate \dot{M}_{Edd}), (iv) size of the corona; shock location (X_s in gravitational radius $r_g = GM_{BH}/c^2$), (v) density jump across the shock; compression ratio ($R = \rho_+/\rho_-$, where ρ_+ and ρ_- represent the densities in the post-shock and pre-shock flows), and (vi) outflow collimation factor (f_{col}), the ratio of the solid angle subtended by the outflow to the inflow (Θ_o/Θ_i). Since the model has BH mass as a free parameter, one can successfully determine its value from the spectral modeling (see Debnath et al. 2014; Molla et al. 2017; Mondal et al. 2024). The model combination reads in XSPEC as: `tbabs*(JeTCAF + ga[5])` for *Resolve* and `tbabs*(TCAF + ga[3])` for *Xtend*.

Given the above model combinations, the *Resolve* spectrum is best-fitted with $\chi^2_{red} = 1.3$ using JeTCAF model for the parameters $M_{BH} = 5.7 \pm 0.8 M_\odot$, $\dot{m}_d = 2.76 \pm 0.21$, $\dot{m}_h = 0.25 \pm 0.06$, $X_s < 12$, $R = 6.52 \pm 1.37$, and $f_{col} = 0.12 \pm 0.03$. The high disk mass accretion compared to the hot sub-Keplerian component infers the soft spectral state. The Keplerian disk moved much closer to the BH $< 12r_g$ (pegged at the lower bound of the parameter space), also associates the effect of cooling due to the high disk accretion rate that cooled the hot corona. Such phenomena have also been observed for other LMBHs studied using the TCAF model (Mondal et al. 2014, 2017; Chatterjee et al. 2021, 2023). The high value of R and low value of f_{col} refer to the low mass outflow (see Chakrabarti 1999; Mondal & Chakrabarti 2021). Similar to other models, N_H obtained from the fit is also high $37.2 \pm 0.2 \times 10^{22} \text{ cm}^{-2}$. Since there are multiple Fe K lines, we have frozen them to their peak energies at 6.62, 6.64, 6.69, 6.85, and 7.1 keV and let their width vary. The best-fitted line width σ for all Fe K lines is $< 0.03 \text{ keV}$. The *Xtend* data equally fits well for a marginal change within error in the JeTCAF model parameter as in *Resolve* with $\chi^2_{red} = 1.2$. The N_H value required for the *Xtend* data fitting is $24.8 \pm 0.1 \times 10^{22} \text{ cm}^{-2}$. The best-fitted model spectra are shown in Figure 3.

The above model fittings help summarize the estimate of the mass of the BH. The `diskbb` model fits determined the mass in the range $8 - 25 M_\odot$ for different values of the disk inclination angle, which is later better constrained by using the `kerrbb` model fit. The estimated mass of the BH turns out to be $\approx 8 - 10 M_\odot$ from the above two models. From the JeTCAF model fits, the mass of the BH comes out to be $\approx 5.7 \pm 0.8 M_\odot$. Combining these three estimates, the most probable mass of the central compact object becomes $7.9 \pm 2.2 M_\odot$.

As the source MAXI J1744-294 showed complex Fe emission features between 6 - 7 keV in the *Resolve* spectrum. The continuum subtracted emission features clearly indicated the presence of a weak Fe $K\alpha$ & blended Fe XXVI and Fe $K\beta$ emission lines. Additionally, strong He α like complex Fe XXV (forbidden and triplet) emission lines between 6.6 - 6.7

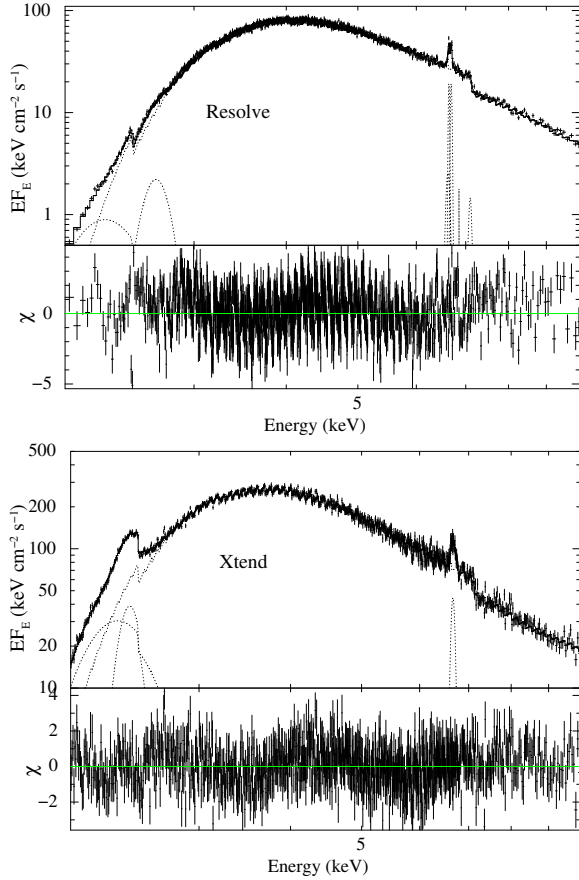


Figure 3. Best-fitted JetCAF model fitted spectra in the 2-10 keV energy band are shown. The top and bottom panels represent the Resolve and Xtend instruments, respectively. The bottom windows of each panel show the residuals of the fits.

keV were detected. So far, we have used phenomenological multiple Gaussian components to fit different Fe K line transitions. However, to produce the line profiles, a realistic emission model is favorable. Therefore, we adopted the publicly available *photemis* model, derived from the *XSTAR* photoionization code. It consists of analytically computed spectra produced by recombined and collisionally ionized plasma.

While fitting the *Resolve* data between 5 - 8 keV, we kept the line of sight N_H and T_{in} fixed to prior obtained values of $16.7 \times 10^{22} \text{ cm}^{-2}$ and 0.62 keV, as they cannot be constrained in the narrow band spectrum. We used the standard pre-calculated ion population of *xstar*, setting all abundances to zero except for iron, which was frozen to 1. The remaining free parameters were ionization parameter ($\log \xi$), turbulent velocity (v_{turb}) and normalization (Norm_{ph}). We found that a combination of three *photemis* components were able to satisfactorily describe the spectral line features between 6-7 keV. The best fit values are presented in Tab 3. The best fitted model decomposition along with residuals is shown in Fig. 4.

Table 3. Best-fit parameters of the photoionization model

Component	$\log \xi$	$v_{turb} \text{ (km s}^{-1}\text{)}$	Norm_{ph}
photemis #1	1.55 ± 0.05	153.29 ± 54.56	1561.36 ± 293.49
photemis #2	3.15 ± 0.05	= #1	94.13 ± 18.48
photemis #3	3.17 ± 0.15	2513.30 ± 206.48	522.95 ± 38.24

The photoionized emission was modeled by a low ionization component ($\log \xi \sim 1.56$) that accounts for Fe $K\alpha$ emission around 6.40 keV and two highly ionized components ($\log \xi \sim 3$) that wholly reproduce the Fe XXV emission complex. We tied the turbulent velocity of two narrow components (photemis #1 and #2) and while keeping the broad component (photemis #3) free during the fit. Our best fitted results indicated that the Fe XXV complex originates from two, comparably ionized plasma of $\log \xi$ 3.15 and 3.17, however showing very distinct velocity widths. The broad component with $v_{turb} = 2513 \text{ km s}^{-1}$ is most likely produced from extremely hot gas located close to the inner edge of accretion disk. The lines are broadened under the effect of Keplerian motion of accretion disk as it extends close to the black hole during the soft spectral state. On the other hand, the narrow component with $v_{turb} = 153 \text{ km s}^{-1}$ is probably the scattered emission from nearby gas that has been strongly photoionized by hard X-ray radiation. Another narrow, low ionized component ($\log \xi \sim 1.6$) fits the weak Fe $K\alpha$ line which originates further away from the accreting source, in much cooler and less dense region.

Since this source is located close to the galactic center, the emission line complex is expected to be contaminated by X-ray diffuse emission from stellar populations in the Galactic bulge and unresolved, accreting magnetic cataclysmic variables (mCVs) (Revnivtsev et al. 2009; Anastasopoulou et al. 2023). This could potentially explain the residuals around ~ 6.7 and 6.8 keV. The persistent narrow emission feature around 6.85 keV does not correspond to any recognized atomic transition. We speculate this could be due to a red-shifted Fe XXVI transition originating from ionized, out-flowing winds. We also noticed clear, broad residuals around 7 keV as well which, most likely is due to the blended emission from Fe XXVI $\text{Ly}\alpha$ and Fe $K\beta$ lines, requiring sophisticated handling of photoionization models, which is beyond the scope of this work.

4. CONCLUSIONS

We have studied the spectral properties of the BHC MAXI J1744-294 after its very first detection in 2025. Using publicly available archived XRISM data on March 03, 2025 (MJD 60737), we have studied the spectrum of the source using both the instruments of this satellite, namely, Resolve and Xtend. The spectacular spectral resolution of the XRISM satellite, especially the Resolve, helps us find the existence

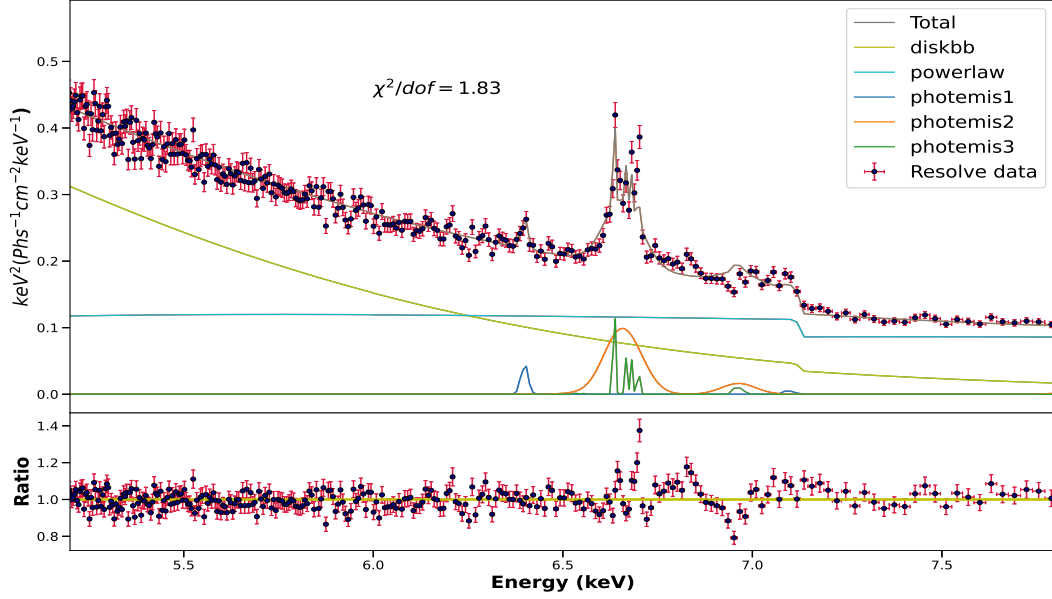


Figure 4. Best fitted *photemis* model fitted to the 5-8 keV *Resolve* spectrum is shown. The top and bottom panels represent the decomposition of model components and residuals respectively.

of multiple iron line profiles in the spectra. In *Xtend*, we also found the existence of an iron line. To take care of the continuum emission, we have used various combinations of some phenomenological and physical models (*diskbb*, *kerbb*, *power-law*, *JeTCAF*, and *photemis*). To take care of the line emissions, we have used multiple lines in the form of the Gaussian model. Along with these, we have used an interstellar absorption model, *tbabs*. We have achieved the best fits with these models. We have also implemented the photoionization modeling in the same spectra using the *photemis* analytic models implemented in *XSPEC*.

From different model fitted results, we conclude that:

- The source was in a soft state at this time of the outburst activity, with the photon index lying in the range of 3.1 – 3.3.
- Different model fitted results suggest that the disk moved much closer to the black hole, with an upper limit of radius $< 12r_g$, and the inner-disk temperature was $T_{in} \sim 0.60 - 0.62$ keV. Additionally, a very high disk accretion rate further supports the soft spectral state during this outburst.
- The detected Fe line complexes from different Fe XXV transitions dominate the 6-7 keV *Resolve* spectrum. The Fe XXV emission arises from two highly ionized plasmas ($\log \xi \sim 3$) with distinct turbulent velocities—one broad ($v_{turb} \approx 2513$ km s⁻¹) from hot gas at the inner accretion disk, and one narrow ($v_{turb} \approx 153$ km s⁻¹) scattered by nearby photoionized gas. A separate low-ionization component ($\log \xi \sim 1.6$) ac-

counts for the weak, narrow Fe K α fluorescent line from cooler, distant regions.

- This is a system in which the disk has a low inclination of $i \sim 24^\circ - 29^\circ$.
- The compact object has a moderate spin $a \sim 0.63 - 0.70$, obtained using the data from both instruments.
- The mass of the black hole is estimated to be $7.9 \pm 2.2 M_\odot$.
- The hydrogen column density is measured to be very high, which could be because the source is situated in a crowded region at the Galactic center.

5. DATA AVAILABILITY

This work has made use of publicly archived data from the XRISM satellite, which is a mission of the Japan Aerospace Exploration Agency in partnership with NASA and ESA. This work has also made use of software from the HEASARC, which is developed and monitored by the Astrophysics Science Division at NASA/GSFC and the High Energy Astrophysics Division of the Smithsonian Astrophysical Observatory.

6. ACKNOWLEDGEMENTS

KC acknowledges support from the SWIFAR postdoctoral fund of Yunnan University. SM acknowledges the Ramanujan Fellowship (# RJF/2020/000113) by SERB/ANRF-DST, Govt. of India, for this research. CBS is supported by the National Natural Science Foundation of China under grant no.

12073021. H.-K. C. acknowledges support from the NSTC project (grant No. 111-2112-M-007-019) of NTHU.

We thank Michael Loewenstein of the University of Maryland, College Park, USA, for his assistance during the data reduction.

REFERENCES

- Anastasopoulou, K., Ponti, G., Sormani, M. C., et al. 2023, *A&A*, 671, A55, doi: [10.1051/0004-6361/202245001](https://doi.org/10.1051/0004-6361/202245001)
- Asai, K., Dotani, T., Nagase, F., & Mitsuda, K. 2000, *ApJS*, 131, 571, doi: [10.1086/317374](https://doi.org/10.1086/317374)
- Belloni, T., Psaltis, D., & van der Klis, M. 2002, *ApJ*, 572, 392, doi: [10.1086/340290](https://doi.org/10.1086/340290)
- Brenneman, L. W., & Reynolds, C. S. 2006, *ApJ*, 652, 1028, doi: [10.1086/508146](https://doi.org/10.1086/508146)
- Casella, P., Belloni, T., & Stella, L. 2005, *ApJ*, 629, 403, doi: [10.1086/431174](https://doi.org/10.1086/431174)
- Chakrabarti, S., & Titarchuk, L. G. 1995, *ApJ*, 455, 623, doi: [10.1086/176610](https://doi.org/10.1086/176610)
- Chakrabarti, S. K. 1999, *A&A*, 351, 185, doi: [10.48550/arXiv.astro-ph/9910014](https://doi.org/10.48550/arXiv.astro-ph/9910014)
- Chakrabarti, S. K., Debnath, D., Nandi, A., & Pal, P. S. 2008, *A&A*, 489, L41, doi: [10.1051/0004-6361:200810136](https://doi.org/10.1051/0004-6361:200810136)
- Chatterjee, K., Debnath, D., Chatterjee, D., Jana, A., & Chakrabarti, S. K. 2020, *MNRAS*, 493, 2452, doi: [10.1093/mnras/staa391](https://doi.org/10.1093/mnras/staa391)
- Chatterjee, K., Debnath, D., Chatterjee, D., et al. 2021, *Ap&SS*, 366, 63, doi: [10.1007/s10509-021-03967-x](https://doi.org/10.1007/s10509-021-03967-x)
- Chatterjee, K., Debnath, D., Nath, S. K., & Chang, H.-K. 2023, *ApJ*, 956, 55, doi: [10.3847/1538-4357/acf463](https://doi.org/10.3847/1538-4357/acf463)
- Chatterjee, K., Mondal, S., Singh, C. B., & Sugizaki, M. 2024a, *ApJ*, 977, 148, doi: [10.3847/1538-4357/ad8dc4](https://doi.org/10.3847/1538-4357/ad8dc4)
- Chatterjee, K., Pujitha Suribhatla, S., Mondal, S., & Singh, C. B. 2024b, *arXiv e-prints*, arXiv:2406.17629, doi: [10.48550/arXiv.2406.17629](https://doi.org/10.48550/arXiv.2406.17629)
- Corbel, S., & Fender, R. P. 2002, *ApJL*, 573, L35, doi: [10.1086/341870](https://doi.org/10.1086/341870)
- Debnath, D., Chakrabarti, S. K., & Mondal, S. 2014, *MNRAS*, 440, L121, doi: [10.1093/mnrasl/slu024](https://doi.org/10.1093/mnrasl/slu024)
- Dhawan, V., Mirabel, I. F., & Rodríguez, L. F. 2000, *ApJ*, 543, 373, doi: [10.1086/317088](https://doi.org/10.1086/317088)
- Done, C., Gierliński, M., & Kubota, A. 2007, *A&A Rv*, 15, 1, doi: [10.1007/s00159-007-0006-1](https://doi.org/10.1007/s00159-007-0006-1)
- Fabian, A. C., Rees, M. J., Stella, L., & White, N. E. 1989, *MNRAS*, 238, 729, doi: [10.1093/mnras/238.3.729](https://doi.org/10.1093/mnras/238.3.729)
- García, J., & Kallman, T. R. 2010, *ApJ*, 718, 695, doi: [10.1088/0004-637X/718/2/695](https://doi.org/10.1088/0004-637X/718/2/695)
- George, I. M., & Fabian, A. C. 1991, *MNRAS*, 249, 352, doi: [10.1093/mnras/249.2.352](https://doi.org/10.1093/mnras/249.2.352)
- Haardt, F., & Maraschi, L. 1993, *ApJ*, 413, 507, doi: [10.1086/173020](https://doi.org/10.1086/173020)
- Heinke, C. O., Nakajima, M., Kudo, Y., et al. 2025, *The Astronomer's Telegram*, 17010, 1
- Iwasawa, K., Fabian, A. C., Reynolds, C. S., et al. 1996, *MNRAS*, 282, 1038, doi: [10.1093/mnras/282.3.1038](https://doi.org/10.1093/mnras/282.3.1038)
- Jaisawal, G. K., Steiner, J. F., Strohmayer, T. E., et al. 2025, *The Astronomer's Telegram*, 17040, 1
- Kubota, A., Tanaka, Y., Makishima, K., et al. 1998, *PASJ*, 50, 667, doi: [10.1093/pasj/50.6.667](https://doi.org/10.1093/pasj/50.6.667)
- Kudo, Y., Negoro, H., Nakajima, M., et al. 2025, *The Astronomer's Telegram*, 16975, 1
- Li, L.-X., Zimmerman, E. R., Narayan, R., & McClintock, J. E. 2005, *ApJS*, 157, 335, doi: [10.1086/428089](https://doi.org/10.1086/428089)
- Majumder, S., Kushwaha, A., Singh, S., et al. 2025, *arXiv e-prints*, arXiv:2506.03774, doi: [10.48550/arXiv.2506.03774](https://doi.org/10.48550/arXiv.2506.03774)
- Mandel, S., Mori, K., Hailey, C., et al. 2025, *The Astronomer's Telegram*, 17063, 1
- Marinucci, A., Matt, G., Miniutti, G., et al. 2014, *ApJ*, 787, 83, doi: [10.1088/0004-637X/787/1/83](https://doi.org/10.1088/0004-637X/787/1/83)
- Marra, L., Mikušincová, R., Vincentelli, F. M., et al. 2025, *arXiv e-prints*, arXiv:2506.17050, doi: [10.48550/arXiv.2506.17050](https://doi.org/10.48550/arXiv.2506.17050)
- Matsuoka, M., Kawasaki, K., Ueno, S., et al. 2009, *PASJ*, 61, 999, doi: [10.1093/pasj/61.5.999](https://doi.org/10.1093/pasj/61.5.999)
- Molla, A. A., Chakrabarti, S. K., Debnath, D., & Mondal, S. 2017, *ApJ*, 834, 88, doi: [10.3847/1538-4357/834/1/88](https://doi.org/10.3847/1538-4357/834/1/88)
- Mondal, S., Adhikari, T. P., & Singh, C. B. 2021, *MNRAS*, 505, 1071, doi: [10.1093/mnras/stab1194](https://doi.org/10.1093/mnras/stab1194)
- Mondal, S., & Chakrabarti, S. K. 2021, *ApJ*, 920, 41, doi: [10.3847/1538-4357/ac14c2](https://doi.org/10.3847/1538-4357/ac14c2)
- Mondal, S., Chakrabarti, S. K., Nagarkoti, S., & Arévalo, P. 2017, *ApJ*, 850, 47, doi: [10.3847/1538-4357/aa7e27](https://doi.org/10.3847/1538-4357/aa7e27)
- Mondal, S., Debnath, D., & Chakrabarti, S. K. 2014, *ApJ*, 786, 4, doi: [10.1088/0004-637X/786/1/4](https://doi.org/10.1088/0004-637X/786/1/4)
- Mondal, S., Suribhatla, S. P., Chatterjee, K., Singh, C. B., & Chatterjee, R. 2024, *ApJ*, 975, 257, doi: [10.3847/1538-4357/ad7d92](https://doi.org/10.3847/1538-4357/ad7d92)
- Motta, S., Muñoz-Darias, T., Casella, P., Belloni, T., & Homan, J. 2011, *MNRAS*, 418, 2292, doi: [10.1111/j.1365-2966.2011.19566.x](https://doi.org/10.1111/j.1365-2966.2011.19566.x)
- Nakajima, M., Negoro, H., Kudo, Y., et al. 2025, *The Astronomer's Telegram*, 16983, 1
- Pozdnyakov, L. A., Sobol, I. M., & Syunyaev, R. A. 1983, *Astrophys. Space Phys. Res.*, 2, 189
- Remillard, R. A., & McClintock, J. E. 2006, *ARA&A*, 44, 49, doi: [10.1146/annurev.astro.44.051905.092532](https://doi.org/10.1146/annurev.astro.44.051905.092532)

- Revnivtsev, M., Sazonov, S., Churazov, E., et al. 2009, *Nature*, 458, 1142, doi: [10.1038/nature07946](https://doi.org/10.1038/nature07946)
- Ross, R. R., & Fabian, A. C. 2005, *MNRAS*, 358, 211, doi: [10.1111/j.1365-2966.2005.08797.x](https://doi.org/10.1111/j.1365-2966.2005.08797.x)
- Shimura, T., & Takahara, F. 1995, *ApJ*, 445, 780, doi: [10.1086/175740](https://doi.org/10.1086/175740)
- Sunyaev, R. A., & Titarchuk, L. G. 1980, *A&A*, 86, 121
- Tashiro, M., Maejima, H., Toda, K., et al. 2021, in *Society of Photo-Optical Instrumentation Engineers (SPIE) Conference Series*, Vol. 11444, Society of Photo-Optical Instrumentation Engineers (SPIE) Conference Series, ed. J.-W. A. den Herder, S. Nikzad, & K. Nakazawa, 1144422, doi: [10.1117/12.2565812](https://doi.org/10.1117/12.2565812)
- Tetarenko, B. E., Sivakoff, G. R., Heinke, C. O., & Gladstone, J. C. 2016, *ApJS*, 222, 15, doi: [10.3847/0067-0049/222/2/15](https://doi.org/10.3847/0067-0049/222/2/15)
- Titarchuk, L., & Shrader, C. 2005, *ApJ*, 623, 362, doi: [10.1086/424918](https://doi.org/10.1086/424918)
- Watanabe, S., Aoyama, A., Takeda, T., et al. 2025, *The Astronomer's Telegram*, 17009, 1

APPENDIX

A. DISKBB+POWERLAW MODEL FITS

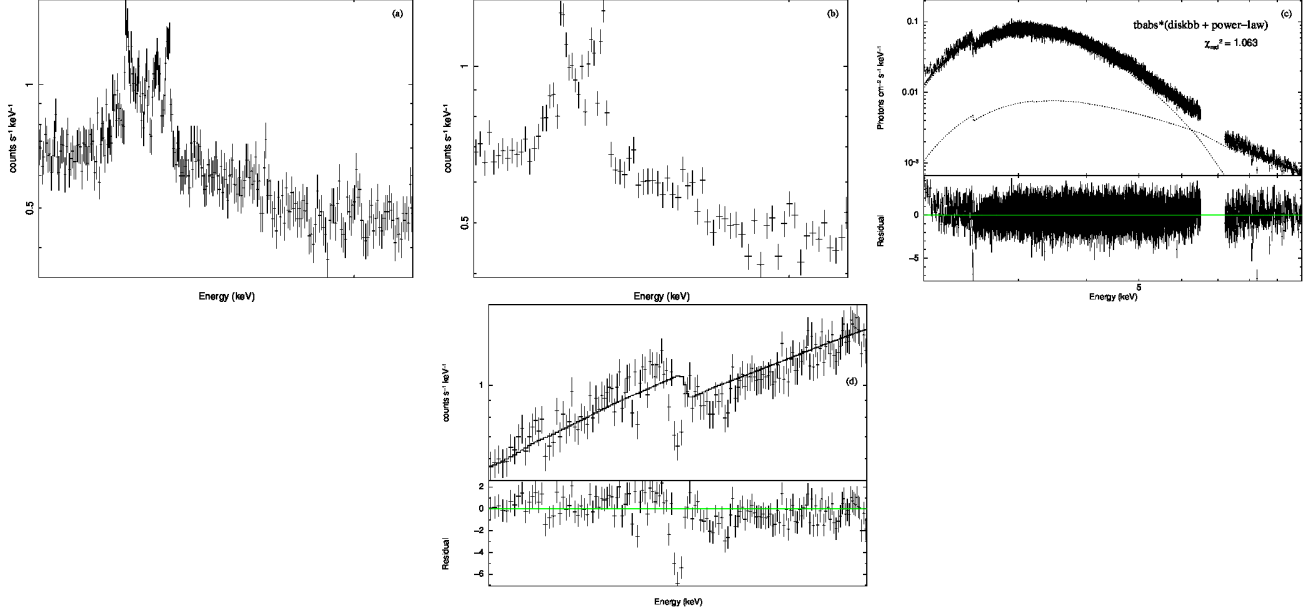


Figure A1. Unanalyzed (panel a-b) and analyzed (panel c-d) resolve spectra. Panels (a & b) are the zoomed-in part of the spectrum in the energy range of 6.5 – 7.1 keV. Panel (b) is the rebinned version of panel (a). Panel (c) represents the fitted continuum in the 2 – 10 keV energy band, ignoring the 6.5 – 7.1 keV region. Panel (d) is the zoomed-in fitted spectrum in the 2.35 – 2.6 keV energy band.

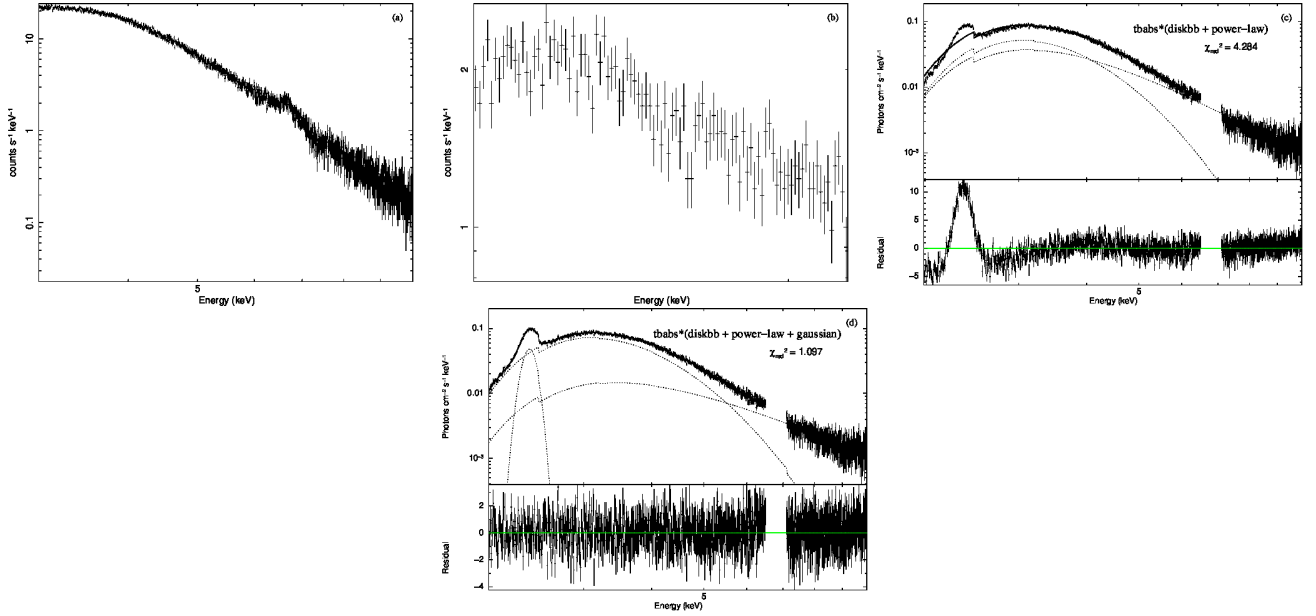


Figure A2. Unanalyzed (panel a-b) and analyzed (panel c-d) xtend spectra. Panels (a & b) are the unfitted continuum and zoomed-in part of the spectrum in the energy range of 6.5 – 7.1 keV. Panels (c & d) represent the fitted continuum in the 2 – 10 keV energy band, ignoring the 6.5 – 7.1 keV region.